



**HAL**  
open science

## Deterministic and Probabilistic Q-Ball Tractography: from Diffusion to Sharp Fiber Distribution

Maxime Descoteaux, Rachid Deriche, Alfred Anwander

► **To cite this version:**

Maxime Descoteaux, Rachid Deriche, Alfred Anwander. Deterministic and Probabilistic Q-Ball Tractography: from Diffusion to Sharp Fiber Distribution. [Research Report] RR-6273, 2007, pp.39. inria-00166299v2

**HAL Id: inria-00166299**

**<https://inria.hal.science/inria-00166299v2>**

Submitted on 29 Aug 2007 (v2), last revised 29 Aug 2007 (v3)

**HAL** is a multi-disciplinary open access archive for the deposit and dissemination of scientific research documents, whether they are published or not. The documents may come from teaching and research institutions in France or abroad, or from public or private research centers.

L'archive ouverte pluridisciplinaire **HAL**, est destinée au dépôt et à la diffusion de documents scientifiques de niveau recherche, publiés ou non, émanant des établissements d'enseignement et de recherche français ou étrangers, des laboratoires publics ou privés.



INSTITUT NATIONAL DE RECHERCHE EN INFORMATIQUE ET EN AUTOMATIQUE

***Deterministic and Probabilistic Q-Ball Tractography:  
from Diffusion to Sharp Fiber Distributions***

Maxime Descoteaux — Rachid Deriche — Alfred Anwander

**N° 6273**

August 2007

Thème BIO



*R*apport  
de recherche





## Deterministic and Probabilistic Q-Ball Tractography: from Diffusion to Sharp Fiber Distributions

Maxime Descoteaux<sup>\*</sup>, Rachid Deriche<sup>†</sup>, Alfred Anwander<sup>‡</sup>

Thème BIO — Systèmes biologiques  
Projet Odysée

Rapport de recherche n° 6273 — August 2007 — 36 pages

**Abstract:** We propose a deterministic and a probabilistic extension of classical diffusion tensor imaging (DTI) tractography algorithms based on a sharp fiber orientation distribution function (ODF) reconstruction from Q-Ball Imaging (QBI). An important contribution of the paper is the integration of some of the latest state-of-the-art high angular resolution diffusion imaging (HARDI) data processing methods to obtain accurate and convincing results of complex fiber bundles with crossing, fanning and branching configurations. First, we develop a new deconvolution *sharpening* transformation from diffusion ODF (dODF) to fiber ODF (fODF). We show that this sharpening transformation improves angular resolution and fiber detection of QBI and thus greatly improves tractography results. The angular resolution of QBI is in fact improved by approximately  $20^\circ$  and the fODF is shown to behave very similarly of the fiber orientation density (FOD) estimated from the spherical deconvolution method of Tournier et al. Another major contribution of the paper is the extensive comparison study on human brain datasets of our new deterministic and probabilistic tracking algorithms. As an application, we show how the reconstruction of transcallosal fiber connections intersecting with the corona radiata and the superior longitudinal fasciculus can be improved with the fODF in a group of 8 subjects. Current DTI based methods neglect these fibers, which might lead to wrong interpretations of the brain functions.

**Key-words:** fiber tractography, diffusion tensor imaging (DTI), high angular resolution diffusion imaging (HARDI), q-ball imaging (QBI), spherical deconvolution (SD), orientation distribution function (ODF)

<sup>\*</sup> Maxime.Descoteaux@sophia.inria.fr

<sup>†</sup> Rachid.Deriche@sophia.inria.fr

<sup>‡</sup> anwander@cbs.mpg.de. Max Planck Institute for Human Cognitive and Brain Science, Leipzig, Germany

## **Déconvolution Sphérique de l'ODF et Tractographie Déterministe et Probabiliste en Imagerie par Q-Ball**

**Résumé :** Nous proposons d'étendre les algorithmes de tractographie classiques développés sur les images de tenseur de diffusion (DTI) pour les appliquer à l'imagerie par Q-Ball (QBI). Une contribution importante de ce rapport est l'intégration de l'état de l'art des méthodes de traitement d'images de diffusion à haute résolution angulaire (HARDI) pour obtenir des réseaux complexes de l'architecture neuronale de la matière blanche comportant des croisements, des embranchements et des configurations en éventail. D'abord, nous développons une nouvelle méthode de déconvolution sphérique pour transformer la fonction de distribution de diffusion des orientations (dODF) en une fonction de distribution d'orientations des fibres (fODF). Cette transformation de *sharpening* augmente la résolution angulaire d'environ  $20^\circ$  et facilite l'extraction des maxima de l'ODF. Par conséquent les résultats de tractographie sur les fODFs sont plus complets et de meilleure qualité. Ensuite, nous démontrons que la fODF et la distribution obtenue par déconvolution sphérique classique de Tournier et al se comportent de la même manière sur des simulations de données HARDI. Enfin, une autre contribution importante du rapport est l'étude poussée et la comparaison des algorithmes de tractographie déterministes et probabilistes sur des données HARDI réelles à partir du DTI, de la dODF et de la fODF. Nous montrons une application intéressante sur le corps calleux et la reconstruction des fibres transcallosales. Ces fibres sont normalement complètement ignorées par les techniques de tractographie en DTI car elles croisent le faisceau supérieur longitudinal ainsi que la couronne rayonnante. Notre tractographie en QBI basée sur la fODF nous permet de retrouver ces fibres transcallosales sur une base de données de 8 sujets, ce qui nous permet une connaissance anatomique plus fine de ces parties du cerveau.

**Mots-clés :** Tractographie, imagerie du tenseur de diffusion (DTI), imagerie de diffusion à haute résolution angulaire (HARDI), imagerie par Q-ball (QBI), fonction de distribution des orientations (ODF), déconvolution sphérique

## Contents

<b>1</b>	<b>Introduction</b>	<b>4</b>
<b>2</b>	<b>Tractography Overview</b>	<b>5</b>
<b>3</b>	<b>Methods</b>	<b>7</b>
3.1	Analytical Regularized ODF from QBI . . . . .	7
3.2	Sharpening and the Fiber ODF . . . . .	8
3.3	Deterministic Multidirectional ODF Tracking . . . . .	9
3.4	Probabilistic fiber ODF Tracking . . . . .	11
3.5	Data Acquisition . . . . .	12
3.5.1	Synthetic Data Generation . . . . .	12
3.5.2	Human Brain Data . . . . .	12
3.6	Evaluation of the Deconvolution Sharpening Transformation . . . . .	13
3.6.1	Spherical Deconvolution . . . . .	13
3.6.2	Synthetic Data Experiment . . . . .	13
3.6.3	Real Data Experiment . . . . .	14
3.6.4	Quantifying the Projections of the Corpus Callosum . . . . .	14
<b>4</b>	<b>Results</b>	<b>17</b>
4.1	Effect of the Deconvolution Sharpening Transformation . . . . .	17
4.2	Tracking . . . . .	20
4.2.1	Deterministic ODF-based Tracking . . . . .	22
4.2.2	Probabilistic Tracking . . . . .	22
4.3	Quantifying Lateral Projections of the Corpus Callosum . . . . .	26
<b>5</b>	<b>Discussion</b>	<b>27</b>
<b>A</b>	<b>Funk-Hecke Theorem</b>	<b>31</b>
<b>B</b>	<b>Diffusion ODF Kernel for Sharpening</b>	<b>31</b>

## 1 Introduction

Diffusion magnetic resonance imaging (MRI) *tractography* is the only non-invasive tool to obtain information on the neural architecture in vivo of the human brain white matter. Tractography is needed to understand functional coupling between cortical regions of the brain and is important for characterization of neuro-degenerative diseases, for surgical planning and for many other medical applications [42]. Currently, white matter fiber tractography is most commonly implemented using the principal diffusion direction of the diffusion tensor (DT) data. The diffusion tensor (DT) model [6] characterizes the orientation dependence of the diffusion probability density function (pdf) of the water molecule. An important limitation of the DT model is the Gaussian diffusion assumption, which implies that there can only be a single fiber population per voxel. At the resolution of DTI acquisitions, this is an important problem since it is known that many voxels have low anisotropy index due to non-Gaussian diffusion coming from multiple fibers crossing, branching, fanning or in a bottleneck. In fact, the resolution of DTI acquisitions is usually between  $3 \text{ mm}^3$  and  $15 \text{ mm}^3$ , while the diameter of bundles of axons considered in fiber tractography are on the order of 1mm and individual physical fibers on the order of 1-30  $\mu\text{m}$  [42]. Thus, tractography algorithms based on the DT can follow false tracts due to diffusion profiles that are prolate or can prematurely stop in regions of isotropic tensors.

To overcome these limitations of the DT, new higher resolution acquisition techniques such as Diffusion Spectrum Imaging (DSI) [57], High Angular Resolution Diffusion Imaging (HARDI) [57], Q-Ball Imaging (QBI) [58] and composite hindered and restricted model of diffusion (CHARMED) [5] have been proposed to estimate the Orientation Distribution Function (ODF) [58] of water molecules. Moreover, other HARDI reconstruction techniques have been proposed to estimate high order spherical functions such as the Persistent Angular Structure (PAS) [30], the Fiber Orientation Density (FOD) [1, 3, 14, 55, 56], the Diffusion Orientation Transform (DOT) [43] and multi-tensor distributions [40, 57]. All these HARDI techniques are developed to deal with non-Gaussian diffusion process and reconstruct spherical functions with potentially multiple maxima aligned with the underlying fiber populations. A good review of all these high order reconstruction techniques can be found in [2, 16].

Hence, one naturally wants to generalize existing DT-based tractography algorithms with HARDI-based techniques to better deal with fiber crossings. In tractography, two families of algorithms exist: deterministic and probabilistic algorithms. Research groups have recently started to generalize both deterministic and probabilistic DT-based tracking algorithms to use some of the HARDI reconstruction methods mentioned above. Popular high order functions used in the literature are the ODF [10, 11, 24, 46, 57], the PAS function [44] and variants of multi-tensor fitting models [8, 23, 36, 49]. The latter techniques show improvement in tracking results where the DT model fits the data poorly and show preliminary fiber bundles with some crossing and branching configurations handled. In this paper, the high order spherical function used is the ODF estimated from QBI because it is model-free and it can be computed analytically, robustly and quickly with our new approach proposed in [18]. The ODF is the basis of our new tracking algorithms.

To illustrate the contributions of our new tracking algorithms, we focus on complex fiber bundles such as projections of callosal fibers to the cortex. These bundles have been studied extensively

in the neuroanatomical and DTI literature (e.g. [28]). The corpus callosum (CC) is involved in the interhemispheric interaction of cortical regions and the reconstruction of fibers connecting the cerebral hemispheres is of major interest for cognitive research and clinical praxis. While DT-based tractography finds fibers passing through the CC connected with the medial/dorsal cortex, lateral and ventral fibers are not found, since these fibers cross the corona radiata and the superior longitudinal fasciculus (SLF). Only a recent study [48] proposed to use a HARDI-based method to reconstruct fibers of the genu and splenium of the CC.

The goal of the paper is thus to integrate the full multidirectional information of a sharp q-ball fiber ODF in both a new deterministic and a new probabilistic tractography algorithm with emphasis on a comparison on real human brain fiber bundles where classical deterministic and probabilistic DT techniques fail. The contributions of the paper are threefold: 1) We first develop a new transformation from diffusion ODF (dODF) to *sharp fiber* ODF (fODF). We show that this transformation improves angular resolution and fiber detection of QBI. 2) We then extensively validate and compare the fODF against the classical FOD estimated from spherical deconvolution [55] on simulations and find similar behaviors between both methods. 3) We last propose a new deterministic and probabilistic tractography algorithm using all the multidirectional information of the sharp fiber ODF. We perform a comparison study of both tracking algorithms on complex fiber bundles of the cerebral anatomy. In particular, we investigate how the reconstruction of transcallosal fiber connections can be improved by the sharp fiber ODF in voxels where fibers cross the corpus callosum. We show, on 8 subjects, areas of the corpus callosum where the new probabilistic tracking finds fibers connecting the ventral and lateral parts of the cortex, fibers currently missed when using DT-based algorithms.

The paper is outlined as follows. In Section 2, we review relevant tractography background literature to illustrate and motivate our new deterministic and probabilistic algorithms. We then review our fast, regularized and analytical ODF estimation [18] in Section 3.1 and develop the deconvolution sharpening transformation that produces the sharp fiber ODF in Section 3.2. The deterministic and probabilistic tractography algorithms are developed in Sections 3.3 and 3.4 respectively. We next present qualitative and quantitative evaluations of the deconvolution sharpening and compare the deterministic and probabilistic tractography algorithms on several complex fiber bundles in Section 4. Finally, we conclude with a discussion of the results and present directions for future work in Section 5.

## 2 Tractography Overview

The most intuitive tracking algorithms are the classical deterministic streamline (STR) tracking algorithms [7, 13, 41] and slightly more complex tensor deflection (TEND) algorithms [38, 59] used in many applications [29]. Many other DT-based streamlines and flow-based approaches also exist. A good review and discussion of DT-based algorithms can be found in [42]. Here, we focus on HARDI-based tractography algorithms.

Recently, [24, 57] have proposed a generalized streamline tracking algorithm based on the principal direction of the diffusion ODF computed from DSI. In [36], a multi-tensor local model of the data is used to extend the fiber assignment by continuous tracking (FACT) [41] algorithm. Moreover, to deal with more complex fiber configurations, [45] extended streamline tracking with a mixture of

Gaussian densities and similarly, [23] recently extended the TEND model with a bi-Gaussian model. Finally, based on the classical diffusion ODF reconstructed from QBI [58] and the very recent regularized version of the diffusion ODF [51], [10] proposes a streamline approach with curvature constraint following all maxima to deal with fibers crossing. In this paper, we propose another extension to streamline tractography based on the full multidirectional information of the sharp fiber ODF. From this sharp fiber ODF, we extract all available maxima and allow for splitting in multiple directions at each step. Not only can the tracking propagate through fiber crossings but it can also deal with fibers fanning and branching.

Existing deterministic HARDI-based techniques mostly show that tracking is improved where the DT model fits the data poorly. However, these deterministic tractography algorithms inherit the classical limitations of deterministic algorithms such as choice of initialization, sensitivity in estimated principal direction and lack of straightforward way to compute statistics on tracts and lack of connectivity information between regions of the brain. To overcome limitations of deterministic tractography, DT-based probabilistic algorithms have been used such as [9, 21, 37, 45, 49]. This also motivates the development of new HARDI-based probabilistic algorithms. Probabilistic algorithms are computationally more expensive than deterministic algorithms but can better deal with partial volume averaging effects and noise uncertainty in underlying fiber direction. Most importantly, the output of the algorithms are usually designed to give a connectivity index measuring how probable two voxels are connected to one another.

HARDI-based probabilistic tractography have recently been published in the literature [8, 44, 46] to generalize several existing DT-based methods. First, in [8] a mixture of Gaussian model is used to extend the probabilistic Bayesian DT-based tracking [9]. In [46], Monte Carlo particles move inside the continuous field of q-ball diffusion ODF and are subject to a trajectory regularization scheme. In [44], an extension to their DT-based approach [45] is also proposed using a Monte Carlo estimation of the white matter geometry. Their implementation is based on PASMRI with a new noise modeling component. Overall, these methods show successful tracking of several fiber bundles difficult to recover with DT-based techniques. The methods have mainly focused on fibers with crossing configurations and have not attempted to account for fibers demonstrating high curvature or points where fiber populations branch or fan. In this paper, our new probabilistic algorithm attempts to account for branching and fanning fiber populations as well as fibers crossing.

Normally, an advantage of the probabilistic tractography techniques is that they are based on the full spherical function considered (DT, ODF, PAS, etc...) and not only on the principal direction or maximum(a) extracted. However, this creates a problem when the spherical function profiles are smooth and have significant isotropic parts. In that case, tractography produces diffusive tracking results that leak into unexpected regions of the white matter. This is a well-known problem in probabilistic DT tractography and has not been thoroughly studied in the literature. Typically, one simply take a power of the diffusion tensor [4, 35, 38, 54] to increase the ratio of largest to smallest eigenvalue and thus have enhanced and more elongated tensors. However, this heuristic transformation can create degenerate tensors with second and/or third null eigenvalue.

To solve this problem of diffusive tracking and leaking in ODF-based tracking methods, one needs to use the fiber ODF to obtain more complete and accurate tracts. The relation between diffusion ODF and fiber ODF is unknown and is currently an open problem in the field [46, 57].

Spherical deconvolution (SD) methods [1, 3, 14, 55] reconstruct such a fiber orientation distribution, the FOD, without the need of the diffusion ODF. However, anybody working with QBI and diffusion ODFs has the problem of dealing with smooth ODFs that have a large diffusion part not aligned with the principal fiber directions. Hence, we propose a new ODF sharpening deconvolution operation which has the desired effect of transforming the diffusion ODF into a sharp fiber ODF and we extensively compare our sharp fiber ODF with the classical FOD estimated from SD [55]. We show that this ODF deconvolution transformation is a natural pre-processing task when one is interested in fiber tracking.

### 3 Methods

In this section, we introduce our analytical solution to QBI developed in [18], our sharpening deconvolution operation transforming the diffusion ODF into a sharp fiber ODF and our new deterministic and probabilistic tracking algorithms.

#### 3.1 Analytical Regularized ODF from QBI

Tuch [57, 58] showed that the ODF could be estimated directly from the raw HARDI measurements on a single sphere by a numerical implementation of the Funk-Radon transform (FRT). We have showed in [18] that this FRT could be solved analytically, robustly, and more quickly. The key idea is to express the HARDI signal as a spherical harmonic (SH) series of order  $\ell$  and to solve the FRT using the Funk-Hecke theorem. Note that Anderson [3] and Hess et al [26] have recently developed independently a similar analytical solution for the ODF reconstruction in QBI. Despite the fact that our analytical solution is similar, our regularized estimation part, the derivation, the experimental results, and the validation phase are quite different and clearly demonstrated in [18].

In our analytical QBI solution, the signal at position  $p$  is first estimated as

$$S(\mathbf{u})_p = \sum_{j=1}^R c_j Y_j(\mathbf{u}), \quad (1)$$

where  $S(\mathbf{u})$  is the measured diffusion weighted signal in each of the  $N$  gradient direction  $\mathbf{u} := (\theta, \phi)$  on the sphere ( $\theta, \phi$  obey physics convention,  $\theta \in [0, \pi], \phi \in [0, 2\pi]$ ),  $c_j$  are the SH coefficients describing the signal,  $Y_j$  is the  $j^{th}$  element of the SH basis and  $R = (1/2)(\ell + 1)(\ell + 2)$  is the number of terms in the basis of order  $\ell$  when choosing only even orders. Our implementation is based on a modified symmetric, real, orthonormal basis and the coefficients  $c_j$  are obtained with a Laplace-Beltrami regularization least-square approach to eliminate unnecessary higher order terms in the SH approximation [17]. Note that this kind of regularization was also applied with success to the FOD estimated with spherical deconvolution in [50] using a gradient constraint instead of a Laplace-Beltrami constraint. The exact Laplace-Beltrami regularized expression for the coefficients  $c_j$  is given in [17, Eq.15]. Our Laplace-Beltrami regularization is using the right operator for the space of functions of the unit sphere and gives better estimation and more robust fiber detection [18] than without regularization [3] or with classical Tikhonov regularization [26].

Spherical harmonics allow the simplification of the Funk-Radon Transform (FRT) by the Funk-Hecke theorem. The final ODF reconstruction,  $\Psi$ , at position  $p$ , is simply a diagonal linear transformation of the signal SH coefficients  $c_j$ ,

$$\Psi(\mathbf{u})_p = \sum_{j=1}^R 2\pi P_{\ell_j}(0) c_j Y_j(\mathbf{u}), \quad (2)$$

where  $\ell_j$  is the order associated with  $j^{\text{th}}$  SH basis element (for  $j = \{1, 2, 3, 4, 5, 6, 7, \dots\}$ ,  $\ell_j = \{0, 2, 2, 2, 2, 2, 4, \dots\}$ ) and  $P_{\ell_j}(0)$  a Legendre polynomial with simple expression since we use only even orders in the SH basis,

$$P_{\ell_j}(0) = (-1)^{\ell_j/2} \left( \frac{3 \cdot 5 \cdots (\ell_j - 1)}{2 \cdot 4 \cdots \ell_j} \right). \quad (3)$$

### 3.2 Sharpening and the Fiber ODF

Anybody working with QBI and/or a diffusion ODF has the problem of dealing with a smooth ODF that has a large diffusion part not aligned with the principal fiber directions. The relation between diffusion ODF and fiber ODF is unknown and is currently an open problem in the field [46, 57]. Here, we describe the sharpening operation that aims to transform this smooth diffusion ODF into a sharp fiber ODF [19].

The sharpening operation is a simple linear transformation of the spherical harmonic (SH) coefficients describing the diffusion ODF. The idea is to use spherical deconvolution. Our approach is inspired by the original spherical deconvolution approach proposed by Tournier et al [55], where the measured signal is expressed as the convolution on the unit sphere of the fiber response function with the fiber orientation density function (FOD) [55, Fig.1]. Assuming a particular fiber response function representing the diffusion signal attenuation that would be measured for a single fiber, [55] shows that the deconvolution of the signal with the response function gives the FOD. This was also recently used by others in [14, 56].

Here, the starting point is not the measured signal but our estimated diffusion ODF described in the previous Section 3.1. We want to deconvolve the estimated smooth diffusion ODF by a certain diffusion ODF kernel for a single fiber in order to obtain a sharpened ODF. The procedure is sketched in Fig. 1. We assume that the estimated diffusion ODF,  $\Psi$ , is formed by convolution between the single fiber diffusion ODF kernel,  $R$ , and the true fiber FOD. Hence, the deconvolution of the diffusion ODF by the diffusion ODF kernel can recover a sharp fiber ODF.

The convolution on the sphere between  $R$  and  $\Psi_{\text{sharp}}$  (Fig. 1a) can be written as

$$\Psi(\mathbf{u}) = \int_{|\mathbf{w}|=1} R(\mathbf{u} \cdot \mathbf{w}) \Psi_{\text{sharp}}(\mathbf{w}) d\mathbf{w}. \quad (4)$$

In order to solve this integral, we first replace  $\Psi$  and  $\Psi_{\text{sharp}}$  with their respective SH estimation of order  $\ell$ ,  $\sum_j c_j Y_j(\mathbf{u})$  and  $\sum_j c_{j_{\text{sharp}}} Y_j(\mathbf{u})$  and obtain

$$\sum_{j=1}^R c_j Y_j(\mathbf{u}) = \sum_{j=1}^R c_{j_{\text{sharp}}} \int_{|\mathbf{w}|=1} R(\mathbf{u} \cdot \mathbf{w}) Y_j(\mathbf{w}) d\mathbf{w}.$$

At this point, we use the Funk-Hecke theorem stated in Appendix A to solve the integral over the sphere between  $R$  and the spherical harmonic  $Y_j$ . The Funk-Hecke formula is a theorem that relates the inner product of any spherical harmonic with any continuous function defined on the interval  $[-1, 1]$ . It was also at the core of our analytical ODF estimation presented in Section 3.1 [18]. Hence, we obtain

$$c_{j_{\text{sharp}}} = \frac{c_j}{f_j}, \quad \text{where} \quad f_j = 2\pi \int_{-1}^1 P_{\ell_j}(t) R(t) dt, \quad (5)$$

$P_{\ell_j}$  is a Legendre polynomial of order  $\ell_j$  and coefficients  $f_j$  come from the Funk-Hecke formula, which is expanded in Eq. 15 of Appendix B. Therefore, the final sharp fiber ODF expression at position  $p$  is given by

$$\Psi_{\text{sharp}}(\mathbf{u})_p = \sum_{j=1}^R 2\pi P_{\ell_j}(0) \frac{c_j}{f_j} Y_j(\mathbf{u}). \quad (6)$$

For the rest of the paper, we define this ODF as the sharp fiber ODF (fODF).

The main consideration is thus the creation of a viable diffusion ODF kernel  $R$ . Assuming that a Gaussian can describe the diffusion of water molecules for a single fiber, we choose a prolate tensor profile with eigenvalues  $e_1 \geq e_2 = e_3$  to represent this Gaussian. Then, using the analytical relation between diffusion tensor and diffusion ODF [18, 58], we obtain our diffusion ODF kernel  $R$ . In the synthetic simulations of [18, 55] and in the model-based approach of [14], values of  $[e_2, e_2, e_1]$  are chosen from physiological data. Here, we prefer to estimate the diffusion ODF kernel directly from our real dataset, as done in Tournier et al [55, 56] for single fiber response function. All details are given in Appendix B, where the analytical diffusion ODF kernel,  $R$ , is derived. In practice, the average prolate tensor profile is estimated from 300 voxels with highest FA value, as these tensors can each be assumed to contain a single fiber population.

### 3.3 Deterministic Multidirectional ODF Tracking

We extend the classical streamline techniques [7, 13, 42] based on diffusion tensor principal direction to take into account multiple ODF maxima at each step. We denote  $p(s)$  as the curve parameterized by its arc-length. This curve can be computed as a 3D path adapting its tangent orientation locally according to vector field  $\mathbf{v}$ . Hence, for a given starting point  $p_0$ , we solve  $p(t) = p_0 + \int_0^t \mathbf{v}(p(s)) ds$ . The integration is typically performed numerically with Euler or Runge-Kutta schemes of order 2 or 4. In the Euler case, we have the discrete evolution equation

$$p_{n+1} = p_n + \mathbf{v}(p_n) \Delta s, \quad (7)$$

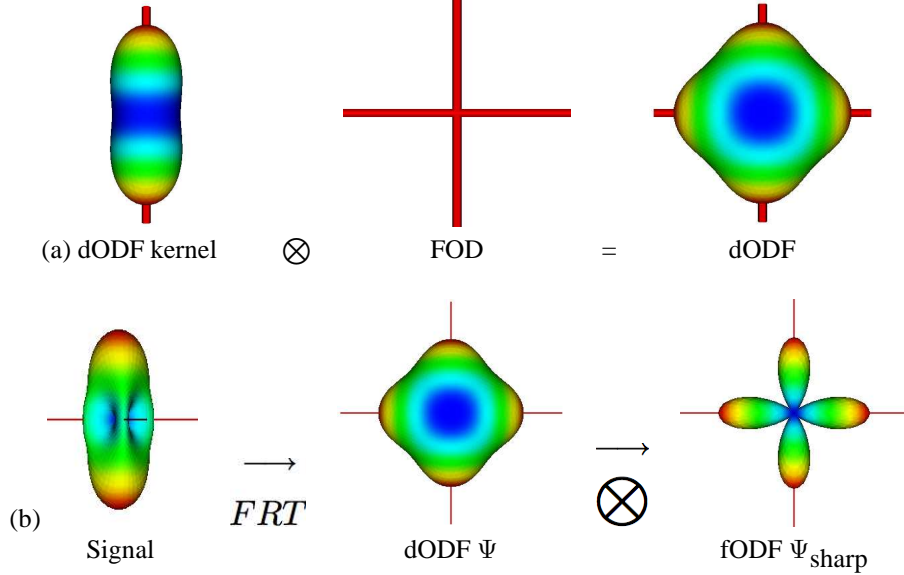


Figure 1: Sketch of the convolution/deconvolution. In (a), the convolution between the diffusion ODF (dODF) kernel and the fiber orientation function (FOD) produces a smooth diffusion ODF. In (b), we show a sketch of the deconvolution sharpening. The Funk-Radon Transform (FRT) of the simulated HARDI signal on the sphere produces a smooth diffusion ODF. This diffusion ODF is transformed into a sharp fiber ODF (fODF) by the deconvolution with the diffusion ODF kernel of (a).

where  $\Delta s$  is a small enough step size to obtain subvoxel precision. A continuous linear, cubic, spline or geodesic [39] interpolation of the vector field can be done at each step for the subvoxel points. A good review is found in [42] and more recently in [11, 25].

For seed point  $p_0$ , for a given anisotropy measure  $A$  that can be FA, Generalized FA (GFA) [58] or any other measure, for anisotropy threshold  $t_{aniso}$ , for curvature threshold  $t_\theta$ , for  $\text{ExtractMax}(\Psi, p)$  a function returning the list  $l$  of vector(s) oriented along each ODF,  $\Psi$ , maximum(a) at point  $p$ , for  $\text{size}(l)$  returning the size of list  $l$  and for  $l_j$  representing the  $j^{\text{th}}$  element of list  $l$ , our algorithm can be described as follows:

- (0) Estimate field of fODF,  $\Psi_{\text{sharp}}$ , with Eq. 6  
(1) **Set** seed  $p_0$  and **set**  $\mathbf{v}(p_0) = \text{argmax}_{\mathbf{u}} \Psi_{\text{sharp}}(\mathbf{u})_{p_0}$   
(2) Update curve according to Eq. 7.  
**If**  $A(p_n) < t_{\text{aniso}}$  **then STOP**;  
**If**  $\frac{\mathbf{v}(p_n) \cdot \mathbf{v}(p_{n-1})}{\|\mathbf{v}(p_n)\| \|\mathbf{v}(p_{n-1})\|} > t_\theta$  **then STOP**;  
**Let**  $l = \text{ExtractMax}(\Psi_{\text{sharp}}, p_n)$ . **If**  $\text{size}(l) > 1$   
**then SPLIT** curve; **for**  $i = 1$  to  $|l|$   
**do** (1) with  $p_0 = p_n$  and  $\mathbf{v}(p_0) = l_i$ ;

ODF estimation is done with order  $\ell = 4, 6$  or  $8$  as in [18] and ODF kernel estimated from our real dataset. To extract ODF maxima, it is generally assumed that they are simply given by the local maxima of the normalized ODF ( $[0,1]$ ), where the function surpasses a certain threshold (here, we use  $0.5$ ). In practice, we project the ODF onto the sphere tessellated with a fine mesh. We use a 16th order tessellation of the icosahedron, which gives 1281 sample directions on the sphere. Then, we implement a finite difference method on the mesh. If a mesh point is above all its neighbors and if this point has an ODF value above  $0.5$ , we keep the mesh point direction as a maxima. This thresholding avoids selecting small peaks that may appear due to noise. Other more complex methods exist to extract the maxima such the method presented in [27] or spherical Newton's method [55].

In our implementation, we use FA and  $t_{\text{aniso}} = 0.1$  as a mask to prevent tracks to leak outside white matter, we set curving angle threshold  $t_\theta = 75^\circ$  and  $\Delta s = 0.1$  and we use Euler integration and classical trilinear interpolation to obtain dODF, fODF and DT at subvoxel precision. For the rest of the paper, DT-STR refers to this algorithm using the DT principal eigenvector, dODF-STR and fODF-STR refers to this algorithm using a single dODF/fODF maxima that is the closest to the incoming tangent direction of the curve, and SPLIT-STR refers to this algorithm using all available fODF maxima with splitting at each step.

### 3.4 Probabilistic fiber ODF Tracking

In this section, we propose an extension of the random walk method proposed by Anwander et al. [4] and Koch et al. [35] to use the multidirectional fiber ODF. Imagine a particle in a seed voxel moving in a random manner with a constant speed within the brain white matter. The transition probability to a neighboring point depends on the local fODF,  $\Psi_{\text{sharp}}$ . This fODF is discretized into 120 directions evenly distributed and at every time step, one of these 120 direction is picked at random according to the fODF distribution. This yields higher transitional probabilities along the main fiber directions. Hence, the particle will move with a higher probability along a fiber direction than perpendicular to it. We start a large number of particles from the same seed point, let the particles move randomly according to the local fODF and count the number of times a voxel is reached by the path of a particle. The random walk is stopped when the particle leaves the white matter volume.

For each elementary transition of the particle, the probability for a movement from the seed point  $x$  to the target point  $y$  in one of the 120 directions  $\mathbf{u}_{xy}$  is computed as the product of the local fODFs in direction  $\mathbf{u}_{xy}$ , i.e.

$$P(x \rightarrow y) = \Psi_{\text{sharp}}(\mathbf{u}_{xy})_x \cdot \Psi_{\text{sharp}}(\mathbf{u}_{xy})_y \quad (8)$$

where  $P(x \rightarrow y)$  is the probability for a transition from point  $x$  to point  $y$  and  $\Psi_{\text{sharp}}(\mathbf{u}_{xy})_x$  is the fiber ODF in point  $x$  in direction  $y$ .

The transition directions in the local model are limited to 120 discrete directions corresponding to the angular sampling resolution of the acquired data, and the step size of the particle step was fixed to 0.5. We used trilinear interpolation of the fODF for the subvoxel position and projected to 120 discrete directions (same as our real data gradient encodings). Moreover, voxels within the CSF and voxels containing mainly gray matter were excluded from the tracking using a mask computed from a minimum FA value of 0.1 and a maximum ADC value of 0.0015. These values were optimized to produce a good agreement with the white matter mask from the T1 anatomy. The mask was morphologically checked for holes in regions of low anisotropy due to crossing fibers. Finally, a total of 100000 particles were tested for each seed voxel. To remove artifacts of the random walk, only voxels which were reached by at least 100 particles were used for further processing. For visualization purposes, the dynamic range of the connectivity values was changed by logarithmic transformation and the entire tractogram was normalized between 0 and 1. For the rest of the paper, the 3-dimensional distribution of connected voxels to the seed voxel is called a *tractogram*.

The main novelties in the probabilistic algorithm compared to previous published versions [4, 35] are the use of the fODF after deconvolution of the diffusion data, the higher angular sampling combined with a continuous interpolation of the data and the subvoxel tracking of the streamline. The deconvolution sharpening pre-processing step is shown to have a dramatic impact on the quality of the tractogram. For the rest of the paper, the method just described is referred to as fODF-PROBA.

## 3.5 Data Acquisition

### 3.5.1 Synthetic Data Generation

We generate synthetic ODF data using the multi-tensor model which is simple and leads to an analytical expression of the ODF [18]. For a given  $b$ -factor and noise level, we generate the diffusion-weighted signal

$$S(\mathbf{u}_i) = \sum_{k=1}^n p_k e^{-b \mathbf{u}_i^T \mathbf{D}_k \mathbf{u}_i} + \text{noise}, \quad (9)$$

where  $\mathbf{u}_i$  is the  $i^{\text{th}}$  gradient direction on the sphere,  $n$  is the number of fibers,  $p_k$  is the volume fraction of the  $k^{\text{th}}$  fiber and  $\mathbf{D}_k$  the  $k^{\text{th}}$  diffusion tensor profile oriented randomly. We use tensor profile  $\mathbf{D}_k$  estimated directly on our real dataset using 300 voxels with highest FA from our real dataset. Finally, we add complex Gaussian noise with standard deviation of  $\sigma$ , producing a signal with signal to noise ratio (SNR) of  $1/\sigma$ .

### 3.5.2 Human Brain Data

Diffusion weighted data and high-resolution T<sub>1</sub>-weighted images were acquired in 8 healthy right-handed volunteers ( $25 \pm 4$  years, 4 females) on a whole-body 3 Tesla Magnetom Trio scanner (Siemens, Erlangen) equipped with an 8-channel head array coil [4]. Written informed consent was obtained from all subjects in accordance with the ethical approval from the University of Leipzig.

The spin-echo echo-planar-imaging sequence, TE = 100 ms, TR = 12 s, 128 x 128 image matrix, FOV = 220 x 220 mm<sup>2</sup>, consists of 60 diffusion encoding gradients [32] with a b-value of 1000 s/mm<sup>2</sup>. Seven images without any diffusion weightings are placed at the beginning of the sequence and after each block of 10 diffusion weighted images as anatomical reference for offline motion correction. The measurement of 72 slices with 1.7mm thickness (no gap) covered the whole brain. Random variations in the data were reduced by averaging 3 acquisitions, resulting in an acquisition time of about 45 minutes. No cardiac gating was employed to limit the acquisition time. The issue of cardiac gating is discussed in [33]. Additionally, fat saturation was employed and we used 6/8 partial Fourier imaging, a Hanning window filtering and parallel acquisition (generalized auto-calibrating partially parallel acquisitions, reduction factor = 2) in the axial plane.

The brain is peeled from the T1-anatomy, which was aligned with the Talairach stereotactical coordinate system [53]. The 21 images without diffusion weightings distributed within the whole sequence were used to estimate motion correction parameters using rigid-body transformations [31], implemented in [22]. The motion correction for the 180 diffusion-weighted images was combined with a global registration to the T1 anatomy computed with the same method. The gradient direction for each volume was corrected using the rotation parameters. The registered images were interpolated to the new reference frame with an isotropic voxel resolution of 1.72 mm and the 3 corresponding acquisitions and gradient directions were averaged.

## 3.6 Evaluation of the Deconvolution Sharpening Transformation

### 3.6.1 Spherical Deconvolution

For comparison with our sharp fODF, we also reconstruct the FOD using spherical deconvolution [55]. We implement the filtered SD (fSD) [55] using spherical harmonics and low-pass filter [1,1,1,0.8,0.1] multiplying each coefficient of order  $\ell \in \{0, 2, 4, 6, 8\}$  respectively (details in [56]). This filtering is introduced to reduce the effect of noise and spurious peaks problem produced by high order spherical harmonic coefficients of the FOD estimation. There are more very recent versions of spherical deconvolution with regularization [50] and positivity constraint with super-resolution [56] that have just appeared in the literature. Here, we choose to compare against the classical fSD [55] because it has been extensively studied in the literature.

### 3.6.2 Synthetic Data Experiment

We evaluate and quantify the angular resolution limitation, the fiber detection success and angular error made on the detected maxima when using the diffusion ODF (dODF) (Eq. 2), the sharp fiber ODF (fODF) (Eq. 6) and the filtered SD (fSD) [55] described in Section 3.6.1. First, to evaluate angular resolution limitations, we generate noise-free synthetic data for two fibers where we vary the crossing angle between fibers to determine the critical angle at which only a single maximum is detected instead of two. Then, to evaluate fiber detection success, we use noisy synthetic data generated with SNR 35 and with 1, 2, or 3 fibers chosen randomly with equal volume fraction and random angle between fibers set above 45°. We generate 1000 such HARDI profile separately and count the number of times we correctly detect the number of ODF maxima. For the simulations,

we also vary estimation order  $\ell = 4, 6$  and  $8$ , use  $b$ -values of  $1000, 3000$  and  $5000 \text{ s/mm}^2$  and use sampling densities of  $N = 81$  and  $321$  on the hemisphere, corresponding to a  $3^{\text{rd}}$  and  $7^{\text{th}}$  order tessellation of the icosahedron respectively. We also record the angular error made in degrees on each direction. Next, to evaluate angular error made on the detected maxima, we fix the fODF and fSD estimation order at  $\ell = 6$  and use a simulation with  $b = 3000 \text{ s/mm}^2$ ,  $N = 60$  (same gradient directions as our real data acquisition), separation angle of  $60^\circ$ ,  $\text{SNR} = 30$  and volume fraction  $p_1 = p_2 = 0.5$ . Finally, we show qualitative simulated results that illustrate the effect of varying HARDI signal generation parameters such as  $b$ -value, SNR, separation angle and volume fraction in Eq. 9.

### 3.6.3 Real Data Experiment

First, we show the effect of the deconvolution sharpening qualitatively on a regions with known fiber crossings between two and three different fiber populations. Then, we compare deterministic tracking methods DT/dODF/fODF/SPLIT-STR and probabilistic dODF/fODF-PROBA on complex fiber bundles. We study the performance of the different algorithms to reconstruct several commissural fiber tracts in one subject. Different seed masks were generated on the color coded FA maps. Fiber tracts and connectivity distributions were generated from every voxel in the mask. For the reconstruction of the fibers passing through the anterior commissure (AC), a seed voxel was placed in the mid-sagittal cross section of the AC and a second tracking was started from two seeds, one on the left and right side of the mid-sagittal cross section; for the commissural fibers connecting the contralateral inferior and middle frontal gyrus a seed voxel was defined in the mid-sagittal section of the rostral body of the CC (Talairach 0, 18, 18); for the tapetum and temporal commissural fibers we selected 4 seed voxels between the left lateral ventricle and the optic radiation close to the splenium of the CC (Talairach -22, -42, 24).

### 3.6.4 Quantifying the Projections of the Corpus Callosum

As an application, we investigated how the reconstruction of transcallosal fiber connections could be improved with the fODF in the group of 8 subjects. We show in which parts of the CC we can reconstruct fibers connecting the ventral and lateral parts of the cortex. These fibers cross the corona radiata and parts of the superior longitudinal fasciculus [53] and cannot be detected with the simple tensor model and are limited with the dODF. Regions of interest (ROIs) for the white matter tractography in each subject were defined by the sagittal cross section of the CC. For each seed voxel in the ROI the fODF-PROBA tractography was performed separately. To evaluate the connectivity to lateral and ventral cortical areas, The percentage of random fiber tracts reaching lateral parts of the brain (Talairach  $> 30$ ) are quantified. The result is color coded on the mid-sagittal plane.

Angular resolution limitations (a)										
		$b = 5000 \text{ s/mm}^2$			$b = 3000 \text{ s/mm}^2$			$b = 1000 \text{ s/mm}^2$		
	order $\ell$	fODF	fSD	dODF	fODF	fSD	dODF	fODF	fSD	dODF
$N = 81$	8	30°	33°	55°	31°	38°	58°	52°	54°	74°
	6	39°	42°	55°	42°	46°	59°	52°	58°	74°
	4	51°	52°	59°	52°	54°	63°	57°	63°	75°
$N = 321$	8	29°	32°	44°	30°	36°	50°	45°	50°	69°
	6	37°	40°	47°	38°	43°	52°	45°	55°	69°
	4	50°	50°	56°	52°	55°	60°	56°	62°	72°
Fiber detection success (b)										
		$b = 5000 \text{ s/mm}^2$			$b = 3000 \text{ s/mm}^2$			$b = 1000 \text{ s/mm}^2$		
	order $\ell$	fODF	fSD	dODF	fODF	fSD	dODF	fODF	fSD	dODF
$N = 81$	8	100%	100%	78%	94%	94%	61%	86%	85%	56%
	6	99%	99%	76%	91%	90%	60%	69%	67%	54%
	4	70%	70%	62%	63%	63%	55%	62%	60%	52%
$N = 321$	8	100%	100%	96%	100%	100%	87%	95%	95%	55%
	6	100%	100%	88%	100%	100%	84%	66%	70%	53%
	4	83%	83%	62%	78%	76%	62%	58%	56%	52%

Table 1: ODF sharpening and spherical deconvolution improve fiber detection and increases angular resolution QBI. The sharp fiber ODF (fODF) and filtered spherical deconvolution (fSD) [55] have similar fiber detection and angular resolution behavior that outperform the classical diffusion ODF (dODF). We test effects of changing estimation order  $\ell$ ,  $b$ -value and spherical sampling density  $N$ . Simulations were done on 1000 HARDI profiles. In (a) HARDI profiles are generated with SNR 35 and with a random number of crossing fibers between 1, 2 and 3 and with random angle between fibers above  $45^\circ$ . In (b), noise-free HARDI simulations are generated with 2 fibers crossing. We report the angle between fibers under which only a single ODF maxima is detected.